ANNEALING EFFECTS ON INTERFACIAL FRACTURE OF GOLD-CHROMIUM FILMS IN HYBRID MICROCIRCUITS

N. R. MOODY, D. P. ADAMS*, A. A. VOLINSKY**, M. D. KRIESE***, W. W. GERBERICH*
Sandia National Laboratories, Livermore, CA 94551-0969, nrmoody@sandia.gov
*Sandia National Laboratories, Albuquerque, NM 87185-0959
**University of Minnesota, Minneapolis, MN 55455
***Osmic Inc., Troy. MI 48084-5532

ABSTRACT

In this study, stressed overlayers and nanoindentation were used to study the effect of elevated temperature on the resistance to interfacial fracture of gold-chromium films in hybrid microcircuits. The samples were prepared by sputter deposition of gold films and chromium adhesive layers onto sapphire substrates. Some films were left in the as-deposited condition for testing. Others were annealed until either most or all the chromium adhesive layer had diffused from the substrate interface. Stressed overlayers and nanoindentation were then used to drive interfacial delamination and blister formation. From these blisters, interfacial fracture energies were determined using mechanics-based models modified for multilayer film effects. The results clearly showed that the chromium interlayers increased interfacial fracture energy. However, they showed an even greater increase in fracture energy after diffusion had reduced the continuous chromium adhesion layer to a solid solution of gold and chromium, suggesting two different mechanisms act to control resistance to interfacial fracture in these films.

INTRODUCTION

Interface structure and composition are two of the most important factors controlling the performance and reliability of thin film devices [1,2]. They are particularly important in gold-chromium hybrid microcircuits which consist of an alumina substrate, a thin chromium layer for adherence, and a gold layer for conductance to connect components on the microcircuit [3-5]. During post deposition processing and service at elevated temperature, diffusion and segregation change the composition and structure of the films and interfaces [3-7]. Nevertheless, the effect of these changes on film adhesion is not well-defined due to limitations in test and analysis techniques [8-10]. These measurements are made even more difficult for the films in hybrid microcircuits as extensive plasticity in ductile films such as gold limits the stress that can be applied at the film-substrate interface [8]. Recent work by Kriese and coworkers [8,10] following the work of Bagchi et al. [11,12] shows that this limitation can be overcome by deposition of a hard highly stressed overlayer. This overlayer applies a uniform stress to the ductile films while constraining out-of-plane plasticity [11-13]. We have therefore conducted a systematic test program to determine how exposure to elevated temperatures during post deposition processing affects susceptibility to fracture of laboratory prepared samples using highly stressed overlayers and nanoindentation to drive delamination and subsequent blister formation. Fracture energies were then determined from these tests using mechanics based models [14-16] modified for bilayer films [8,11,12]. The results clearly show that the use of chromium as an adhesion layer and post-deposition processing at elevated temperatures enhance adhesion. However, the mechanisms differ. In as-deposited samples a continuous chromium layer promotes adhesion. In contrast,

diffusion has reduced this layer to a solid solution of gold and chromium in the annealed samples suggesting that the increase in fracture energies stems from enhanced plasticity at the interface crack tip.

MATERIALS AND PROCEDURE

Materials

In this study, thin gold and gold-on-chromium films were sputter deposited onto polished single crystal (0001) sapphire substrates using a d. c. magnetron sputtering unit. The substrates were prepared by ultrasonic cleaning in acetone for ten minutes, in ethyl alcohol for five minutes, and then in 1M HCl for five minutes. This was followed by rinses with deionized water and nitrogen gas. They were then transferred to the deposition chamber and heated to 700°C in vacuum for five minutes to drive off moisture and cooled to room temperature. Within a vacuum apparatus having a base pressure of 1.3×10^{-5} Pa (10^{-7} Torr), the films were deposited on the substrates using chromium and gold targets, and argon as the carrier gas. Chromium was first deposited on three substrates to a thickness of 6 nm. This was followed by gold deposition to a thickness of 200 nm. Both were deposited at a nominal rate of 0.3 nm/s. A sapphire substrate was added to the gold deposition run to create a gold-on-sapphire film system for reference. The gold-on-chromium film samples were then divided into three groups. One sample was left in the as-deposited condition. A second sample was heated at 400°C for 8 hours in air at which point the continuous chromium layer had begun to come off the sapphire interface in many regions. The third sample was then heated at 400°C for 16 hours in air at which point the continuous chromium layer had been completely reduced to a solid solution of gold and chromium. During heating, chromium had diffused through the gold film to the surface forming Cr_2O_3 upon exposure to air. This oxide was removed using a solution of ceric ammonium nitrate.

Following nanoindentation testing for mechanical properties, a tantalum nitride (Ta_2N) overlayer was deposited on all films to provide a uniform compressive stress for fracture testing. Deposition was accomplished by placing the gold and gold-on-chromium films in the sputter deposition chamber and heating to 170°C in vacuum to drive off moisture. Cleaning was completed with an RF backsputter to remove contaminants from the surface. Within a vacuum system having a base pressure of 1.3×10^{-5} Pa (10^{-7} Torr), the tantalum nitride films were deposited at a rate of 0.3 nm/s using a tantalum target, argon as a carrier gas, and controlled additions of nitrogen. 450 nm-thick Ta_2N overlayers were sputtered on the as-deposited and annealed gold-on-chromium films. A thinner overlayer 275 nm thick was deposited on the pure gold film to explore the minimal stress needed to cause buckling when chromium was not present.

Fracture Testing

Resistance to fracture was determined from uniform width blisters which formed on deposition of the tantalum nitride overlayers, and from circular blisters triggered by nanoindentation of regions where uniform-width blisters did not form. For the nanoindentation tests, a conical diamond indenter with a nominal one µm tip radius and a 90° included angle was driven into the films at a loading rate of 600 µN/s to maximum loads of 25, 50, 100, 200, 400, and 600 mN. During each test, the normal loads and displacements were continuously recorded.

M5.2.2

RESULTS

Film Properties

The chromium adhesive layers were 6 nm thick while the gold layers deposited on sapphire and on chromium were 200 nm thick. Thickness was measured using a Tencor Profilometer and confirmed by Scanning Auger Microscopy. As Figure 1a shows, the as-deposited gold-chromium films consisted of distinct gold and chromium layers with no evidence of significant interdiffusion. In contrast, long term annealing has led to complete depletion of the continuous chromium adhesive layer creating a near uniform through thickness gold-chromium solid solution as shown in Figure 1b. The partially annealed sample had some interface regions where the chromium layer remained continuous and many regions where diffusion had reduced the chromium layer to a gold-chromium solid solution.

The tantalum nitride overlayers on the Gold-chromium films were characterized using a Rigaku X-ray diffraction (XRD) system with a thin film detection system and Cu-Kα radiation. The patterns showed a randomly oriented polycrystalline structure for these overlayers, typical for sputter deposited tantalum nitride. Out-of-plane strain, indicated by shifts in the 2θ peak position for (101), (110), and (211) planes, was then used to calculate the in-plane residual stress assuming isotropic elasticity [17-19]. This gave a value of -2.5 GPa which was subsequently duplicated using an inclined angle method for measuring residual stress [19].

Uniform Width Blisters

Deposition of the tantalum nitride overlayer triggered extensive delamination and telephone cord blistering that completely covered the as-deposited gold film sample surface and one-quarter of the gold-on-chromium film sample surface as shown in Figure 2. There was no

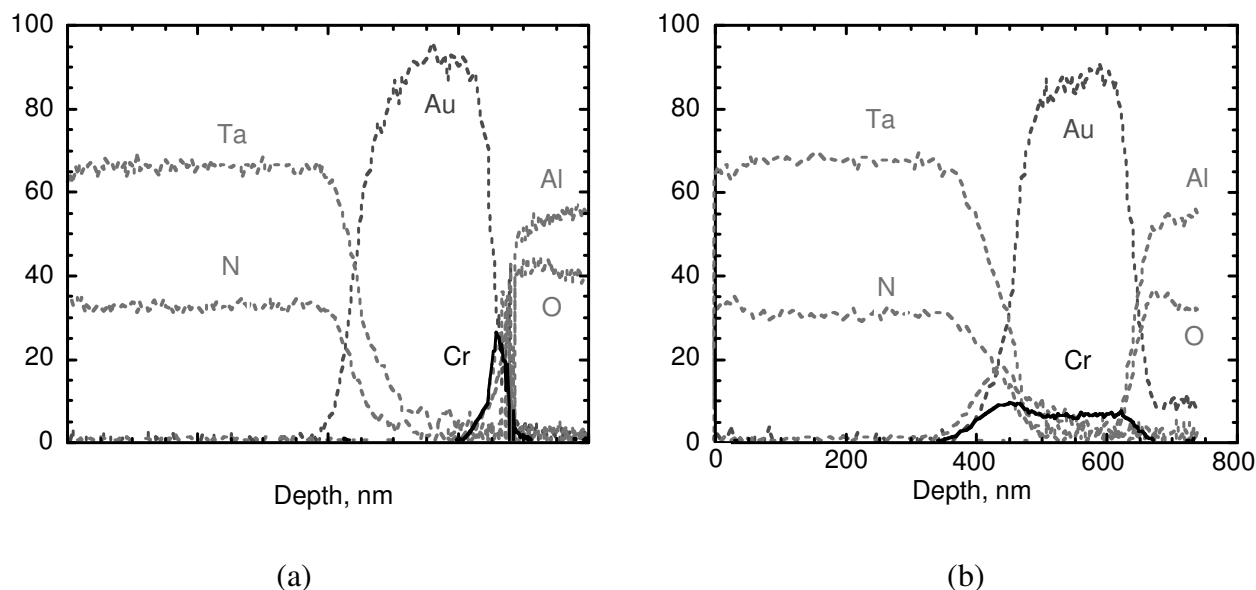
(a)   (b)

Figure 1. Composition profiles of the (a) as-deposited and (b) fully annealed films show that diffusion during annealing has reduced the chromium adhesive layer to a gold-chromium solid solution along the interface.

<center>(a)   (b)</center>
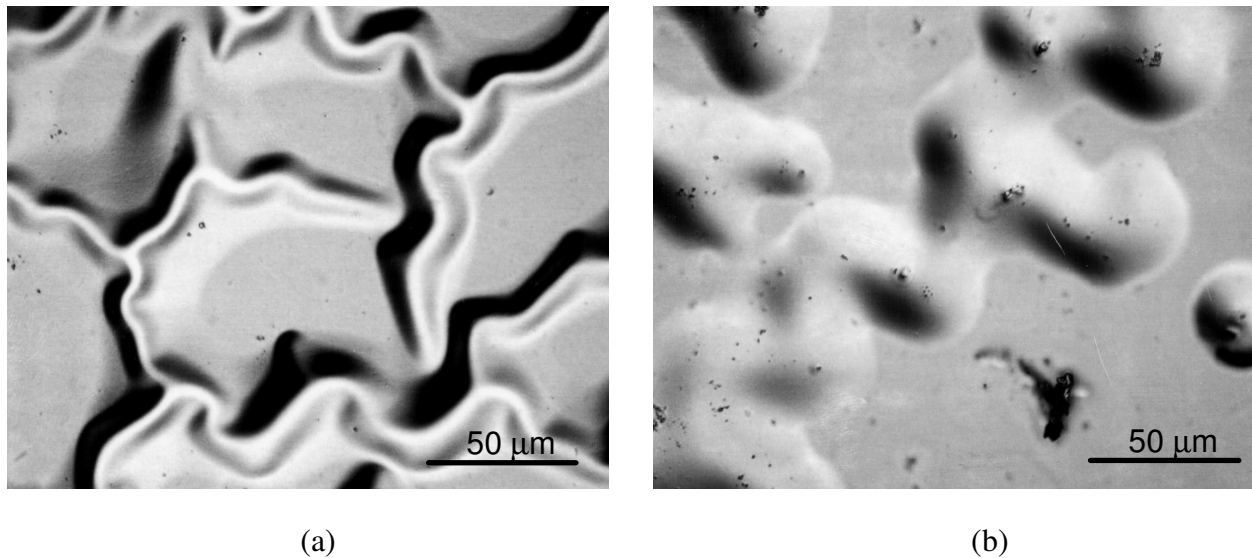
Figure 2. Deposition of the highly stressed tantalum nitride overlayer triggered telephone cord blistering over the entire (a) gold film and over one-quarter of the (b) gold-on-chromium film.

evidence of telephone cord blistering in either the partially or fully annealed film samples. The blistered material readily flaked away exposing the lower fracture surface. High resolution SEM coupled with energy dispersive spectroscopy revealed that fracture had occurred along the film-sapphire interface. The freshly exposed sapphire surface was visually smooth at 50kX with no evidence of chromium or gold. The removal of the blistered film also enabled direct measurement of total film thickness from which it was determined that the tantalum nitride overlayer was 275 nm thick on the gold film and 450 nm thick on the gold-chromium film.
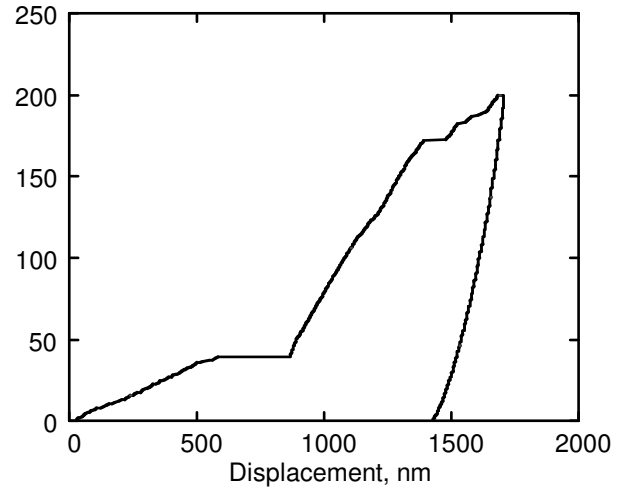
Circular Blisters

Nanoindentation was then used to induce interfacial fracture in the annealed films and the portion of the as-deposited film where telephone cord blistering did not occur. During indentation tests on the as-deposited gold-chromium films, fracture occurred in all tests where the maximum loads exceeded 25 mN, producing large circular spalls as shown in Figure 3a. The onset of fracture is defined by the rapid excursion of the indenter through the films to the sapphire substrate at essentially constant load as shown in Figure 3b. In all cases, fracture occurred by reverse or double buckle formation during indentation with the material under the indenter pinned to the substrate [9]. Increased loading led to additional but smaller excursions, as shown in Figure 3b and larger blister diameters. Eventually annular cracks formed around the indenter at maximum blister height and at the furthest reaches of crack advance where the growing crack kinked in the films. The loads for the onset of fracture in all tests on the as-deposited films were quite uniform in magnitude as shown in Figure 4.

The partially annealed and fully annealed film samples exhibited similar behavior but at higher loads. This is also shown in Figure 4 where the average loads at the onset of fracture were somewhat higher for the partially annealed film and much higher for the fully annealed film than measured in the as-deposited film. However, the fully annealed film exhibited a large degree of scatter indicating that a wide variation in resistance for interface crack nucleation.

<center>M5.2.4</center>
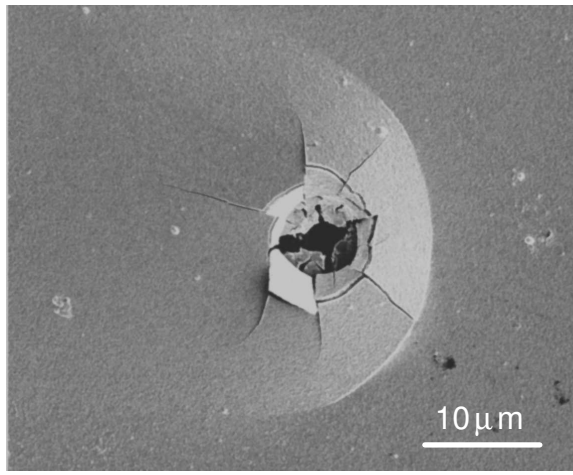
(a)   (b)

Figure 3. (a) Nanoindentation triggered circular blister formation. (b) The onset of fracture is readily defined by the large excursion the load-displacement curve at relatively low loads. The short excursions at high loads correspond to small spurts of crack growth.

FRACTURE ANALYSIS

The uniform width and circular blisters provide the data from which interfacial fracture energies can be obtained using solutions for film systems where residual stresses dominate fracture behavior. These solutions were originally derived for single layer film-on-substrate systems [14-16]. The analysis is based on the assumption that the film and substrate are elastic isotropic solids, the film is subject to a uniform, equibiaxial compressive in-plane stress and the film thickness is much less than the buckle width or diameter. Work by Bagchi et al. [11,12] and more recently by Kriese et al. [8] extended these solutions to multilayer systems by treating the multilayer film as a single film of the same total thickness with a transformed moment of inertia. The single layer film solutions are then multiplied by the ratio of transformed to single layer moment with account taken for the differences in elastic constants, thickness, and residual stress of each layer and their contribution to the total strain energy of the system.

<u>Uniform Width Blisters</u>

The uniform width blister is modeled as a wide, clamped Euler column of width 2b for a blister to form between the multilayer film and substrate under these conditions, the compressive residual stress, σ_r, must exceed the stress for delamination, σ_b, as follows [8,14],

$$\sigma_b = \frac{\pi^2}{Bh\,b^2}\left[\frac{E_{Au}}{(1-\nu_{Au}^2)}\right](I_T) \tag{1}$$

In this expression, I_T is the transformed moment of inertia [8], ν_{Au}, is Poisson's ratio for gold, b is the blister half-width, h is the total film thickness, and B is the unit width, which cancels when multiplied by the transformed moment of inertia [8]. The residual stress can then be determined from the blister height and the stress for delamination as follows [14],

M5.2.5

$$\sigma_r = \sigma_b \left(\frac{3\delta^2}{4h^2} + 1 \right) \qquad (2)$$

where δ is the buckle height and [8],

$$\sigma_r = \sigma_{r_{Au}} \left(\frac{h_{Au}}{h} \right) + \sigma_{r_{Ta_2N}} \left(\frac{h_{Ta_2N}}{h} \right) \qquad (3)$$

Using profilometry, the blister heights and widths were measured on the gold and gold-on-chromium films. Combining these measurements with thickness-weighted elastic moduli and Poisson's ratios, compressive residual stresses of -1.9 and -2.0 GPa were calculated for the tantalum nitride films on gold and gold-on-chromium films respectively and are given in Table I. The good agreement with a directly measured value of -2.5 GPa from x-ray diffraction validates the application of this approach for determining interfacial fracture energies in the gold and gold-on-chromium film systems.

The residual stress and stress for delamination was then used to determine the strain energy release rate for interfacial fracture along the straight side wall portions of the blisters using

$$\Gamma_{I\text{-}II} = \left[\frac{(1-\bar{\nu}^2)h}{2\bar{E}} \right] (\sigma_r - \sigma_b)(\sigma_r + 3\sigma_b) \qquad (4)$$

where $\bar{E}$ and $\bar{\nu}$ are the thickness-weighted elastic modulus and Poisson's ratio values for the multilayer film. Under steady state conditions the width of the blister remains fixed creating the straight-sided blister configuration with growth occurring along the more or less
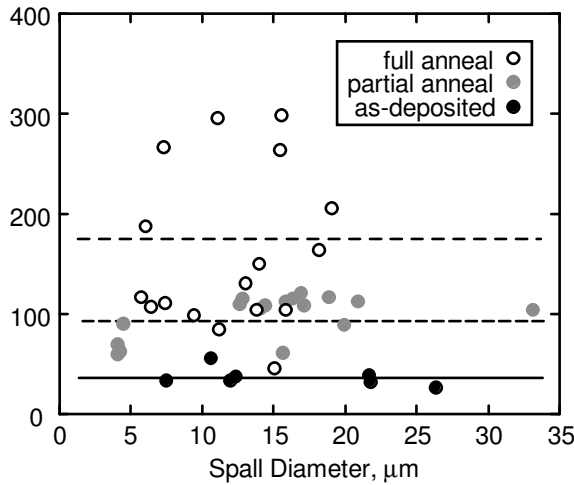

Figure 4. Loads at first fracture are significantly higher in the annealed films and correspond to a greater resistance to interfacial film fracture.
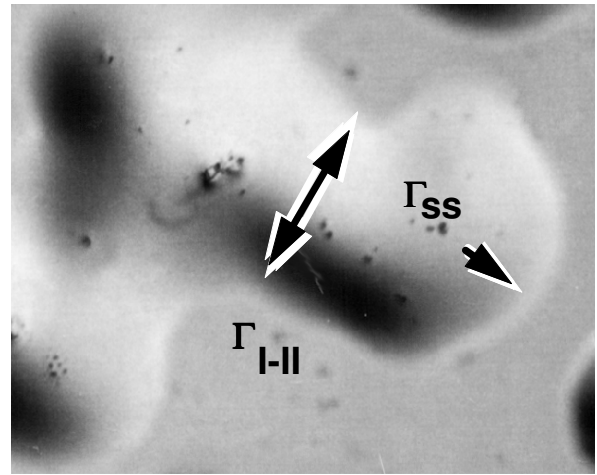

Figure 5. Straight side wall, $\Gamma_{I\text{-}II}$, and steady state, Γ_{ss}, curved front growth locations.

M5.2.6

Table I. Average heights and widths, delamination stresses, residual stresses, and fracture energies of uniform width blisters in as-deposited gold and gold-chromium films.

	h_{Au}	h_{Ta_2N}	b	δ	σ_b	σ_r bilayer	σ_r Ta_2N	Γ_{I-II}	Γ_{ss}
	(nm)	(nm)	(μm)	(μm)	(GPa)	(GPa)	(GPa)	(J/m^2)	(J/m^2)
Au/Al$_2$O$_3$	200	275	14.6	1.3	0.18	-1.1	-1.9	2.1	1.4
Au-Cr/Al$_2$O$_3$	200	450	28.9	2.8	0.09	-1.4	-2.0	3.6	2.9

circular end of the blister. Under these conditions, the steady state fracture energy is given by

$$\Gamma_{ss} = \left[\frac{(1-\bar{v}^2)h\sigma_r^2}{2\bar{E}} \right] \left(1 - \frac{\sigma_b}{\sigma_r} \right)^2 \tag{5}$$

Figure 5 shows Γ_{I-II} and Γ_{ss} fracture locations. The measured straight wall and steady state fracture energies are given in Table I where it is clear that chromium has enhanced film adhesion.

Interfacial Fracture

Interfacial fracture is often treated as a mode I failure with mode I energies at crack arrest set equal to the practical work of adhesion [14,20]. However, the relationship that provides absolute values for mode I and mode II contributions is not well-defined. Nevertheless, several criteria have been proposed to characterize interfacial fracture energy based on the phase angle of loading. Of the criteria proposed, the following two are often observed to bracket the data [14],

$$\Gamma_I = \Gamma_{I-II} \left[1 + (\lambda - 1)\sin^2\psi \right] \tag{6}$$

$$\Gamma_I = \Gamma_{I-II} / \left[1 + (1 - \lambda)\tan^2\psi \right] \tag{7}$$

In these equations, λ is a material parameter equal to 0.3 for most materials, and ψ is the phase angle of loading. It should be noted that significant reservations have been raised concerning determination of the phase angle for multilayer systems [8]. Nevertheless, a phase angle corresponding to crack arrest along the curved front of the telephone cord and circular blisters can be obtained using numerical solutions for circular blister formation by Hutchinson and Suo [14] as follows,

$$\psi = \tan^{-1}(\cos\omega + \frac{h\Delta N}{\sqrt{12}\,M}\sin\omega) / (-\sin\omega + \frac{h\Delta N}{\sqrt{12}\,M}\cos\omega) \tag{8}$$

In this equation, ?N is the in-plane stress, M is the bending moment, and ω is a dimensionless function describing the elastic mismatch between the film and the substrate. The value for h?N/(v12 M) is determined from numerical solutions based on an effective loading parameter, σ_r/σ_c, where σ_c is the delamination stress for a circular blister with a radius defined by

M5.2.7

the telephone cord blister half-width [14]. Ignoring the effect of elastic mismatch between gold and sapphire, which has only a small effect on phase angle for these film systems, ω is set equal to 52.1°. The straight walled portions of the telephone cord blisters are in a state of pure shear. However, the crack front during steady state crack growth reached crack arrest under mixed mode conditions with a strong mode II contribution as shown by the phase angles of loading given in Table II. Mode I contributions were then determined using the criteria given by equations (6) and (7). As Table II also shows, the values from the sine-squared criterion are significantly higher than from the tangent-squared criterion. Of the values from these two criterion, the sine-squared values appear most appropriate for describing adhesion of these films. The value of 0.5 J/m^2 for the gold film is in good agreement with previous work for vacuum deposited gold on soda lime glass [21]. Moreover, only the sine-squared criterion gives values consistent with observations of better adhesion in gold-chromium films.

Indentation Fracture

In the regions of the as-deposited gold-chromium films that did not blister on deposition of the Ta$_2$N overlayer and all portions of the annealed films, nanoindentation was used to trigger delamination and blister formation. In all blisters, the center is constrained giving rise to a reverse or double buckle configuration. For small buckling deflections, Marshall and Evans [15] and Evans and Hutchinson [16] derived an asymptotic solution for strain energy release rate by modeling the blister as a clamped circular plate with a radius much greater than the film thickness and subject to an equibiaxial compressive stress. The compressive stress includes a contribution form indentation. Assuming a rigid substrate and that all material displaced during indentation goes into the film, the stress from indentation is [9,15,16],

$$\sigma_v = \frac{\bar{E} \Delta V}{2 \pi (1 - \bar{\nu}) a^2 h} \tag{9}$$

Previous work [9] on Ta$_2$N Films shows that 60 percent of displaced indent volume contributes to in-plane stresses. For blisters to form during indentation, the total compressive stress from indentation and residual stress must exceed the stress for delamination given by [9,15,16],

$$\sigma_c = \frac{k}{Bh \, a^2} \left[\frac{E_{Au}}{(1 - \nu_{Au}^2)} \right] (I_T) \tag{10}$$

where the constant k equals 42.67 for a circular clamped plate.

Table II. Average steady state fracture energies, phase angles of loading, and corresponding mode I contributions calculated using equations (6) and (7) for uniform width blisters in gold and gold-chromium films.

	Γ_{ss} (J/m^2)	ψ	$\Gamma_{I\text{-}II}/[1+(1-\lambda)\tan^2\psi]$ (J/m^2)	$\Gamma_{I\text{-}II}[(+(\lambda-1)\sin^2\psi]$ (J/m^2)
Au/Al$_2$O$_3$	1.4-72.4	0.18	0.52	
Au-Cr/Al$_2$O$_3$	2.9	-80.2	0.12	0.96

When the film buckles during indentation, the tensile stresses at the edge of the circular crack drive crack advance. Marshall and Evans [15] have derived the strain energy release rate for a circular blister due to residual and indentation stresses. At crack arrest, the strain energy release rate equals the fracture energy as follows,

$$\Gamma_{I-II} = \frac{(1-\bar{v}^2)h\sigma_v^2}{2\bar{E}} + (1-\alpha)\frac{(1-\bar{v})h\sigma_r^2}{2\bar{E}} - (1-\alpha)\frac{(1-\bar{v})(\sigma_v-\sigma_c)}{\bar{E}\sigma_v^2}$$

(11)

where $\alpha=1-[1+0.902(1-v)]^{-1}$ [14]. In the absence of indentation stresses, Hutchinson and Suo [14] have shown that equation is valid only for σ_r/σ_c ratios up to three. Beyond this value, more accurate solutions using the finite difference method have been derived [14].

As-deposited films. During indentation testing, fracture occurred in all tests where maximum loads exceeded 25 mN producing large circular spalls. The spall size increased with increasing test load due to an increase in volume displacement. However, the actual conditions for the onset of crack growth cannot be determined as the tests cannot be stopped during the rapid excursion of the indenter into the film. In a like manner, we cannot factor out contributions to fracture energy from annular and radial cracking or changes from in-plane volume displacements during buckling. Nevertheless, determination of fracture energies corresponding to these two extremes provide upper and lower bounds to the actual mixed mode fracture energies for the as-deposited film. These fracture energies are shown as a function of spall diameter in Figure 6a and are listed in Table III. The large increase in fracture energy at the small spall sizes results from crack interactions with the indenter [22]. The lower limit reached at the largest spall diameters represents the actual fracture energy required for interfacial failure.

Corresponding mode I values were calculated using the criterion given by equation (6). These values are given in Figure 6b and Table III and show the same dependence on spall size as
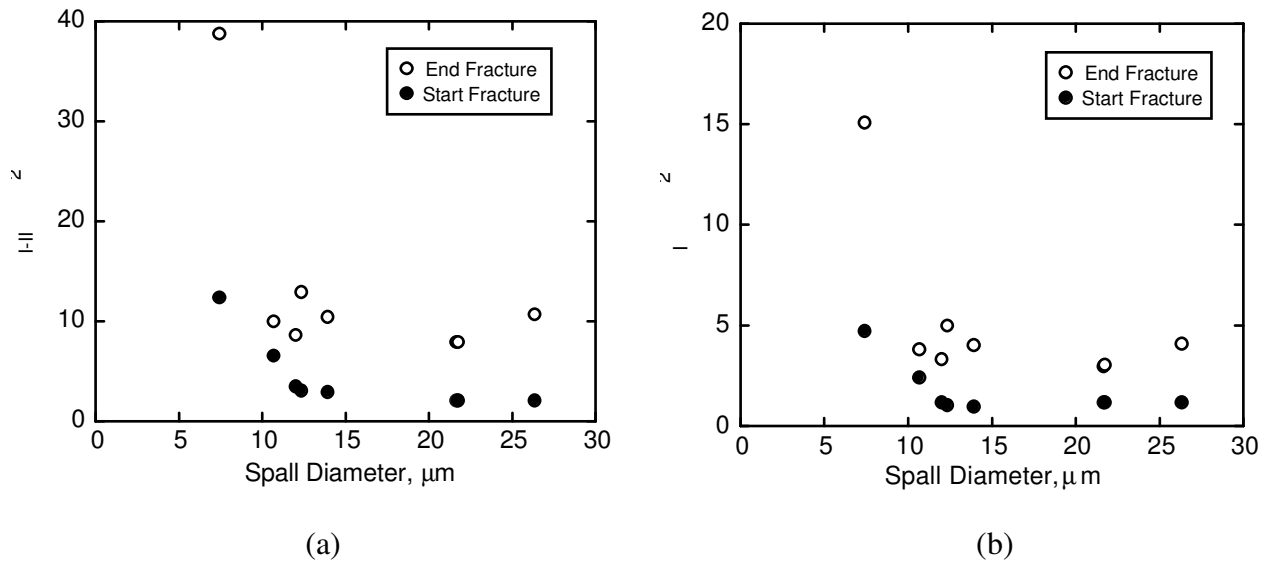

(a)   (b)

Figure 6. (a) Mixed mode and corresponding (b) mode I fracture energies reach a lower liming value for spalls with diameters exceeding 10 μm with values for thestart and end of fracture events providing upper and lower bounds. The mode I values were determined using the sine-squared criterion.

Table III. Average mixed mode I-II start and finish fracture energies, phase angles of loading and corresponding mode I start and finish fracture energies for circular blisters in as-deposited and annealed gold-chromium films.

	$\Gamma_{I\text{-}II}$ (start) (J/m^2)	$\Gamma_{I\text{-}II}$ (finish) (J/m^2)	ψ (J/m^2)	Γ_I (start) (J/m^2)	Γ_I (finsh) (J/m^2)
as-deposited	3.2	9.8	-75	1.1	3.7
partially annealed	5.5	18.2	-72	2.1	7.0
fully annealed	4.9	19.0	-75	1.8	7.3

the mixed mode values. The lower limiting mixed mode and mode I values bracket a range of fracture energies slightly higher than defined by the telephone card blisters. This is consistent with the observation that the portion of the as-deposited film that did not exhibit telephone cord blistering is more strongly adhered to the substrate.

Annealed Films. The annealed films exhibited no evidence of delamination or spontaneous blistering on deposition of the stressed Ta_2N overlayer. In addition, the loads at the onset of fracture were higher and spall sizes smaller for the annealed films when compared to the as-deposited films. The mixed mode I-II fracture energies were then determined for the annealed films using equation (11) and corresponding mode I fracture energies from equation (6). These values are plotted in Figure 7 and are listed in Table III where the partially annealed and fully annealed sample fracture energies overlap for all spall sizes. With only two exceptions for the partially annealed film, these values are significantly greater than exhibited by the as-deposited films. Moreover, for any given spall size, a much greater indentation stress contribution is required for interfacial fracture. Clearly, the resistance to fracture is greater for the annealed films.
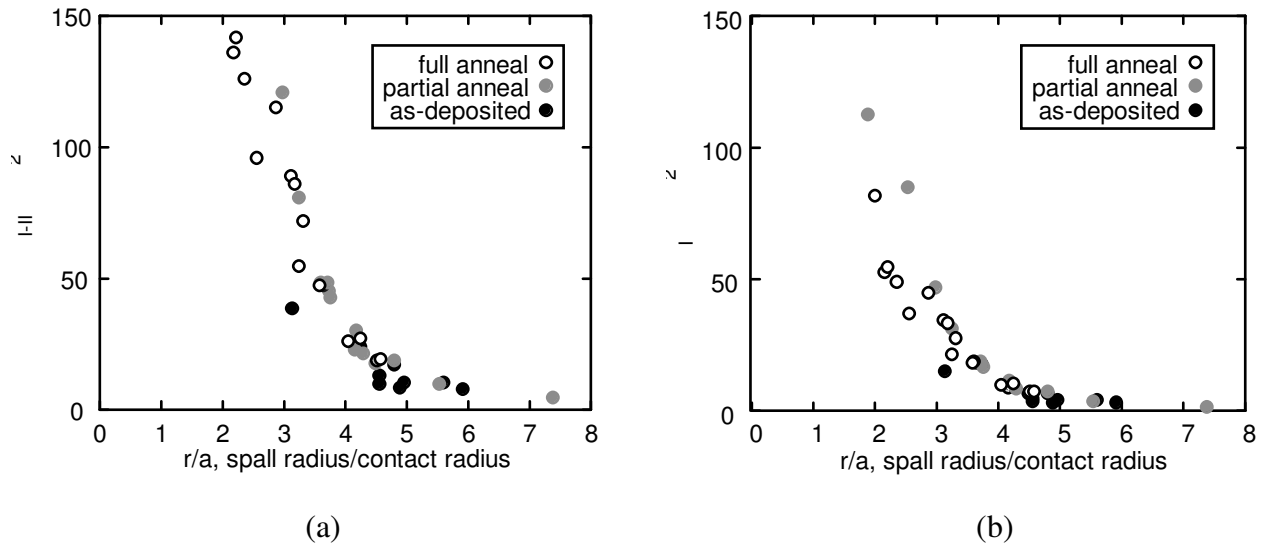

(a)   (b)

Figure 7. (a) Mixed mode and (b) corresponding mode I fracture energies for partially and fully annealed samples overlap for all spall sizes. With only two exceptions, they are significantly higher than values for the as-deposited films.

This increase in fracture energy occurred even though diffusion had reduced much of the chromium adhesion layer in the partially annealed sample and all of the chromium layer in the fully annealed sample to a gold-chromium solid solution. It is unlikely that chromium in solid solution along the interface would promote adhesion over a continuous chromium layer but it will promote plastic deformation beyond that observed for a continuous chromium film. The result is an increase in measured fracture energies as observed in previous work [22] and in this study.

CONCLUSIONS

In this study, highly compressed overlayers were combined with nanoindentation to study the effects of elevated temperature during post deposition annealing on susceptibility to interfacial fracture of gold and gold-chromium films used in hybrid microcircuits. Deposition of highly compressed overlayers induced extensive telephone cord blistering over all of the gold and a portion of the gold-chromium as-deposited films. Fracture occurred exclusively along the as-deposited film-substrate interfaces with no evidence of gold or chromium left on the sapphire substrates. Application of a mechanics based model for steady state growth of uniform width blisters modified for multiple layer films shows that resistance to interfacial fracture of gold-chromium films is significantly higher than for gold films. Nanoindentation was then used to induce fracture of the portion of the as-deposited gold-chromium that did not exhibit telephone cord blistering and in the annealed films. This triggered circular blister formation from which fracture energies were also determined. For the as-deposited film, these values were somewhat higher than measured from the telephone cord blisters, consistent with greater resistance to interfacial fracture. The annealed samples exhibited an even greater increase in resistance to fracture even though diffusion had depleted the chromium adhesion layer. This increase in measured fracture resistance is most likely due to an increase in plastic deformation.

ACKNOWLEDGMENTS

REFERENCES

1. K. L. Mittal, Electrocomponent Science and Technology, **3**, 21 (1976).
2. D. M. Mattox, Thin Solid Films, **18**, p. 173-186 (1973).
3. A. Munitz and Y. Komem, Thin Solid Films, **37**, 171 (1976).
4. R. E. Thomas and G. A. Haas, J. Appl. Phys., **43**, 4900 (1972)
5. J. R. Rairden, C. A. Neugebaur, and R. A. Sigsbee, Metall. Trans., **2**, 719 (1971).
6. M. A. George, W. S. Glaunsinger, T. Thundat, and S. M. Lindsay, Thin Solid Films, **189**, 59 (1990).
7. A. Munitz and Y. Komem, Thin Solid Films, **71**, 177 (1980).
8. M. D. Kriese, W. W. Gerberich, and N. R. Moody, J. Mater. Res., **14**, 3007 (1999).
9. N. R. Moody, R. Q. Hwang, S. Venkataraman, J. E. Angelo, D. P. Norwood, and W. W. Gerberich, Acta mater, **46**, p. 585 (1998).
10 M. D. Kriese, N. R. Moody, and W. W. Gerberich, Acta mater., **46**, 6623 (1998).
11. A. Bagchi and A. G. Evans, Thin Solid Films, **286**, 203 (1996).
12. A. Bagchi, G. E. Lucas, Z. Suo, and A. G. Evans, J. Mater. Res., **9**, 1734 (1994).
13. M. Y. He, A. G. Evans, and J. W. Hutchinson, Acta Metall. Mater., **44,** 2963 (1996).

14. J. W. Hutchinson and Z. Suo, in Advances in Applied Mechanics, edited by J. W. Hutchinson and T. Y. Wu (Academic Press Inc., vol. **29**, New York 1992) pp. 63-191.
15. D. B. Marshall and A. G. Evans, J. Appl. Phys., **56**, 2632 (1984).
16. A. G. Evans and J. W. Hutchinson, Int. J. Solids Struct., **20**, 455 (1984).
17. N. R. Moody, D. Medlin, D. Boehme, and D. P. Norwood, Engng. Fract. Mech., **61**, 107 (1998).
18. R. C. Sun, T. C. Tisone, P. D. Cruzan, J. Appl. Phys., **46**, 112 (1975).
19. B. D. Cullity, *Elements of X-Ray Difffraction*, (Addison-Wesley Publishing Co., Reading, MA, 1956) p. 431.
20. A. G. Evans, M. Ruhle, B. J. Dalgleish, and P. G. Charalambides, in Metal-Ceramic Interfaces, edited by M. Ruhle, A. G. Evans, M. F. Ashby, and J. P. Hirth (Pergammon Press, Oxford, 1990) p. 345.
21. B. N. Chapman, Aspects of Adhesion, vol. **6**, edited by D. J. Alner (U. London Press, London, 1971) p. 43; cited by C. Weaver, J. Vac. Sci. Technol., **12**, 18 (1975).
22. A. A. Volinsky, N. I. Tymiak, M. D. Kriese, W. W. Gerberich, and J. W. Hutchinson, in *Fracture and Ductile vs. Brittle Behavior-Theory, Modeling, and Experiment*, (Mater.. Res. Soc. Proc., **539**, Pittsburgh, PA, 1999) pp. 277-290.